

Article

Improvement of Ferroelectricity in Ce-Doped $\text{Hf}_{0.5}\text{Zr}_{0.5}\text{O}_2$ Thin Films

Yong-Guang Xiao^{1,2,*}, Si-Wei Liu^{1,2}, Li-Sha Yang^{1,2}, Yong Jiang^{1,2}, Ke Xiong^{1,2}, Gang Li^{1,2}, Jun Ouyang^{1,2} and Ming-Hua Tang^{1,2}

¹ Key Laboratory of Key Film Materials & Application for Equipments (Hunan Province), School of Material Sciences and Engineering, Xiangtan University, Xiangtan 411105, China

² Hunan Provincial Key Laboratory of Thin Film Materials and Devices, School of Material Sciences and Engineering, Xiangtan University, Xiangtan 411105, China

* Correspondence: ygxiao@xtu.edu.cn

Abstract: At present, ion doping is a popular method typically used to regulate the ferroelectric properties of $\text{Hf}_{0.5}\text{Zr}_{0.5}\text{O}_2$ films. In this work, Ce (cerium)-doped $\text{Hf}_{0.5}\text{Zr}_{0.5}\text{O}_2$ (Ce: HZO) films on Pt/TiN/SiO₂/Si substrates were prepared by the chemical solution deposition (CSD) method. The microstructure and ferroelectric properties of the Ce-doped HZO films were investigated in detail. The experimental results showed that the remanent polarization value of the films with cerium doping concentration of 7 mol% reached 17 $\mu\text{C}/\text{cm}^2$, which is a significant improvement compared with the undoped $\text{Hf}_{0.5}\text{Zr}_{0.5}\text{O}_2$ films. The reason for this may be the introduction of cerium ions, which can introduce a certain number of oxygen vacancies, thus stabilizing the formation of the orthogonal phase. Interestingly, the films were shown to be nearly fatigue free after 10⁹ cycles of testing. These results demonstrate that cerium ion doping is an effective method for stabilizing the formation of the orthogonal phase of HZO films, and improving the ferroelectricity of HZO thin films.

Keywords: $\text{Hf}_{0.5}\text{Zr}_{0.5}\text{O}_2$ films; orthogonal phases; remanent polarization; endurance



Citation: Xiao, Y.-G.; Liu, S.-W.; Yang, L.-S.; Jiang, Y.; Xiong, K.; Li, G.; Ouyang, J.; Tang, M.-H.

Improvement of Ferroelectricity in Ce-Doped $\text{Hf}_{0.5}\text{Zr}_{0.5}\text{O}_2$ Thin Films. *Coatings* **2022**, *12*, 1766. <https://doi.org/10.3390/coatings12111766>

Academic Editor: Christian Mitterer

Received: 14 October 2022

Accepted: 16 November 2022

Published: 18 November 2022

Publisher's Note: MDPI stays neutral with regard to jurisdictional claims in published maps and institutional affiliations.



Copyright: © 2022 by the authors. Licensee MDPI, Basel, Switzerland. This article is an open access article distributed under the terms and conditions of the Creative Commons Attribution (CC BY) license (<https://creativecommons.org/licenses/by/4.0/>).

1. Introduction

In the past, hafnium dioxide has typically been used as a high-*k* dielectric in state-of-the-art complementary metal-oxide-semiconductor devices [1,2]. However, since the discovery that hafnium oxide doped with silicon has ferroelectric properties [3], it has attracted great attention because of its chemical simplicity, good compatibility with CMOS processes, and excellent scalability [4,5]. In recent years, HfO_2 thin films doped with elements such as Y [6], Al [7], Zr [8], Sr [9], etc., showing good ferroelectric properties, have been reported. At the same time, scholars have carried out a lot of exploratory work retarding the origins of ferroelectricity of hafnium oxide [10–12]. It is generally believed that the ferroelectricity originates from the metastable orthorhombic phase (o-phase: $Pca2_1$). However, the steady phase is the paraelectric monoclinic phase (m-phase: $P2_1/c$). To obtain the steady ferroelectric o phase under normal conditions, many methods have been developed to stabilize the ferroelectric o phase, such as through doping elements [13,14], using flexible substrates [15,16], optimizing the annealing process [17,18], implementing special electrode materials [19,20], selecting crystal orientation [21], etc.

Among the many hafnium-based ferroelectric thin films, HZO ferroelectric thin film is the most promising choice for the application of ferroelectric memory. A lot of optimization work has been carried out with respect to its ferroelectric properties. For instance, Maxim et al. [22] fabricated La: HZO films, and a high remanent polarization value ($2P_r = 30 \mu\text{C}/\text{cm}^2$) and excellent durability with 4×10^{10} endurance cycle tests were obtained. Mohit et al. [23] prepared Y: HZO films, and the experimental results showed that the doping of yttrium helped to introduce oxygen vacancies, stabilizing the ferroelectric o phase, and improving the remanent polarization value. In addition, Yin et al. [24] also

improved the ferroelectricity and durability through a small concentration of Sr doping. The results showed that Sr doping increased the grain size of HZO films, thereby reducing the grain boundaries between grains and reducing the leakage current. Compared with undoped HZO films, the microstructure and ferroelectric properties of the doped hafnium zirconium oxide thin films were significantly improved by ion regulation.

In a previous report [25], HZO films were successfully prepared by a solution method. However, the films exhibited a low remanent polarization of $8 \mu\text{C}/\text{cm}^2$ and a rough surface. Recently, Shiraishi et al. [10] and Künneth et al. [26] reported that Ce element is an excellent dopant that is helpful in regulating the microstructure and improving the ferroelectric properties of hafnium oxide thin films. In the present work, we report Ce doping in $\text{Hf}_{0.5}\text{Zr}_{0.5}\text{O}_2$ films, and different Ce concentrations (0 mol%, 2 mol%, 5 mol%, 7 mol%, 9 mol%) HZO thin films are fabricated by chemical solution deposition method on Pt/Ti/SiO₂/Si substrates. The effects of cerium content on the microstructure and ferroelectric properties of HZO films are systematically investigated. The results demonstrate that improvement of ferroelectric polarization can be realized in CeO₂-HZO solid solution thin films.

2. Experimental Procedure

The experimental process is presented in Figure 1. Hafnium acetylacetonate, zirconium acetylacetonate, acetylacetonate, acetic acid and cerium nitrate were used to prepare precursor solutions. The concentration of the precursor solution was 0.1 mol/L, and the ambient humidity was kept between 10% and 30%. The weighed hafnium source, zirconium source (the mole ratio of hafnium source to hafnium source was 0.5:0.5) and cerium source were poured into the sample bottle. Then, the acetic acid and acetylacetonate with a volume ratio of 4:1 were added to the sample bottle. The obtained mixed solution was then heated and stirred in the water bath for 2 h with the temperature at 55–60 °C so as to facilitate the dissolution of cerium nitrate particles. After stirring, it was left for 72 h, then the precursor solution was filtered, before being packaged and stored in order to obtain the desired solution.

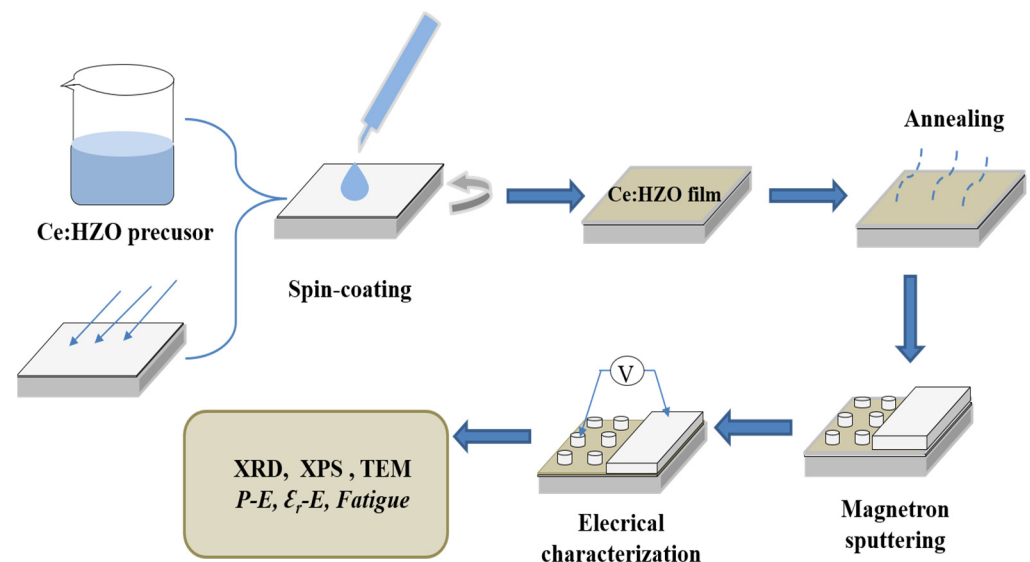


Figure 1. Schematic diagram of the experimental process.

The substrate we used was Pt (111)/TiN/SiO₂/Si (100), with a sheet resistance of 0.001–0.005 Ω/cm. The substrate was cleaned using the standard RCA process. Before preparing the films, the surface was wiped with ethanol to ensure that the substrate surface was clean. The prepared precursor was dropped in the center of the substrate, and rotated at 500 rpm for 15 s and 3000 rpm for 30 s, respectively, to obtain a layer of thin film, which was then dried at 180 °C for 3 min and 400 °C for 5 min. Then, the thin film was annealed in an N₂ atmosphere by raising the temperature to 800 °C for 150 s, and then cooling to

room temperature. Finally, a block electrode and a point electrode of Pt were plated on the thin film using an ion sputtering apparatus (GSL1100X-SPC-12, made by Hefei Jinke, Hefei, China), and the radius and the thickness of the point electrode were 100 μm and about 30 nm, respectively. It should be noted that the point electrode was prepared by means of a mask. When the ion sputtering instrument was powered on, the target splashed atoms in all directions under the action of voltage, and the atoms fell on the surface of the sample, which was covered with a mask to form the point electrodes. The phase of the films were analyzed using Grazing-angle incident X-ray diffraction (GIXRD, Neofconfucianism Ultima IV, Tokyo, Japanese). The chemical composition and valence state of the film surface species were obtained by X-ray photoelectron spectroscopy (XPS, Thermo Scientific K-Alpha, Waltham, MA, USA). The structure of the film was characterized by high-resolution transmission electron microscopy (HRTEM, FEI Talos F200X, Hillsboro, OR, USA). The ferroelectric and dielectric properties of the films were measured using a TF3000 Analyzer and a semiconductor analyzer (Agilent B1500A, Agilent Technologies, CA, America).

3. Results

3.1. Microstructure Characterization of Ce: HZO Films

Figure 2a demonstrates the XRD pattern of Ce: HZO films, with all films being annealed at 800 $^{\circ}\text{C}$. It can be observed that the films show phase transitions with increasing cerium doping concentrations. A relatively prominent diffraction peak can be seen at $2\theta = 30.4^{\circ}$. This peak corresponds to the (111) plane of o/t phase; although it is difficult to identify the specific phase due to their similar lattice parameters, this peak can still provide information for the identification of the structural evolution in the phase transition process [27–29]. Figure 2b shows that when the doping concentration changes from 0 mol% to 7 mol%, the diffraction peak of the ferroelectric o phase gradually increases, and the ferroelectric o phase potentially becomes dominant. However, when the cerium doping concentration reaches 9 mol%, the diffraction peak of (111)_t is enhanced compared with the case of 7 mol%, indicating an increase in the tetragonal phase. Meanwhile, the diffraction peak of (111)_o becomes weak, indicating a decrease in the ferroelectric o phase. Theoretical studies have shown that the use of an appropriate ion doping concentration can reduce the relative free energy of the m phase and the metastable o phase of HfO₂ and ZrO₂, thus realizing the stable formation of o phase [30]. However, the diffraction peaks at 31.7° for (111)_m and 35.2° for (020)_m are very weak for all doping concentrations, and change only slightly. For the doping concentration of 0 mol%, the (−111)_m diffraction peak at 26.8° is more obvious, which is suppressed with increasing doping concentration.

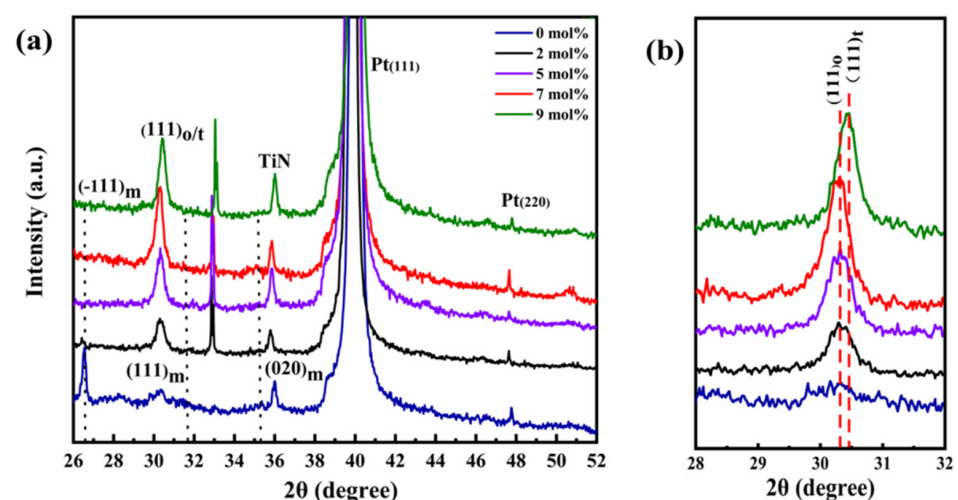


Figure 2. (a) GIXRD of different doping concentrations films; (b) zoomed-in view of the main peak from 28° to 32° .

The chemical states and bonding environments of Ce: HZO films can be directly understood through analysis using X-ray photoelectron spectroscopy. Figure 3a presents the high-resolution XPS spectrum of Hf 4f. The bimodal peak positions of Hf 4f for the 7 mol% sample are at 16.8 eV and 18.5 eV, respectively, which can be attributed to Hf 4f_{7/2} and Hf 4f_{5/2}, respectively, corresponding to the +4 valence state of hafnium in HfO₂ [31]. The binding energy at about 530 eV in Figure 3b is related to the lattice oxygen, indicating the formation of Hf–O bonds, Zr–O bonds and Ce–O bonds [27]. Meanwhile, the higher binding energy at about 532 eV corresponds to non-lattice oxygen. The presence of non-lattice oxygen can be attributed to the overlapping of the surface hydroxyl groups and oxygen vacancies, but it is difficult to distinguish their contributions [28,32]. With regard to oxygen vacancies, they may be introduced when Hf⁴⁺ is replaced by Ce³⁺, similar to what occurs in Y-HfO₂ ferroelectric films [33]. Figure 3c shows the XPS spectra of Ce³⁺ and Ce⁴⁺. Figure 3d presents the XPS survey spectra of 7 mol% Ce-doped films without the impurity peak. It can be observed from Figure 3a,b that the bond energy of both Hf 4f and O1s increases with increasing doping concentration, which may be related to the increase in oxygen vacancy concentration in the thin film. In a study on La: HfO₂ [34], it was reported that the films with pure oxygen vacancies on the surface were able to inhibit the formation of the m phase, while a large number of oxygen vacancies caused the ferroelectric properties of the films to disappear, and a moderate oxygen vacancy concentration contributed to the stabilization of the ferroelectric o phase.

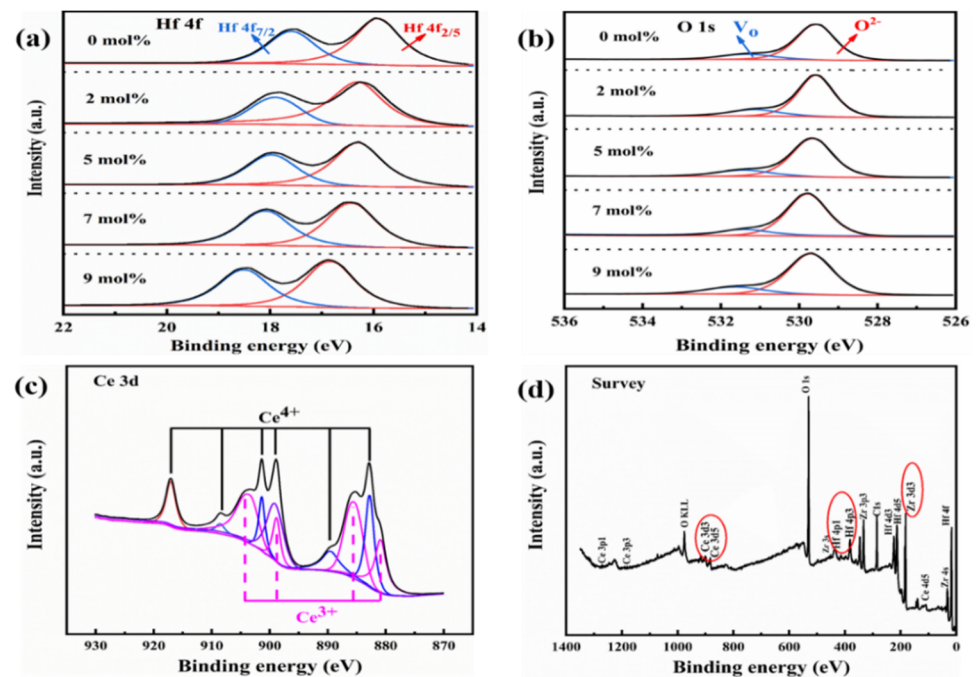


Figure 3. (a) High-resolution XPS spectra of Hf 4f and (b) O 1s core level with different Ce concentrations; (c) Ce 3d and (d) XPS survey spectra of 7 mol% Ce-doped films.

Figure 4a reveals the cross-sectional transmission electron microscope (TEM) images of the 7 mol% Ce: HZO metal–ferroelectric–metal (MIM) structure. To improve the conductivity during the test, a gold layer was deposited on platinum. It can be seen that the thickness of the Ce: HZO film was 20 nm. An enlarged HRTEM image is shown in Figure 4b. The two selected regions are marked with a yellow frame and an orange frame, respectively. Fast Fourier transform (FFT) was performed to obtain the phase structure; the inter-plane distance of the yellow frame was about 2.94 Å and the orange frame was 2.54 Å [35,36], corresponding to the (111)_o and (020)_m planes, respectively. It can be seen that the proportion of o phase in the thin film was much more than that of the m phase.

Combined with XRD and the electrical properties (described below), the stable formation of ferroelectric o phase can be confirmed.

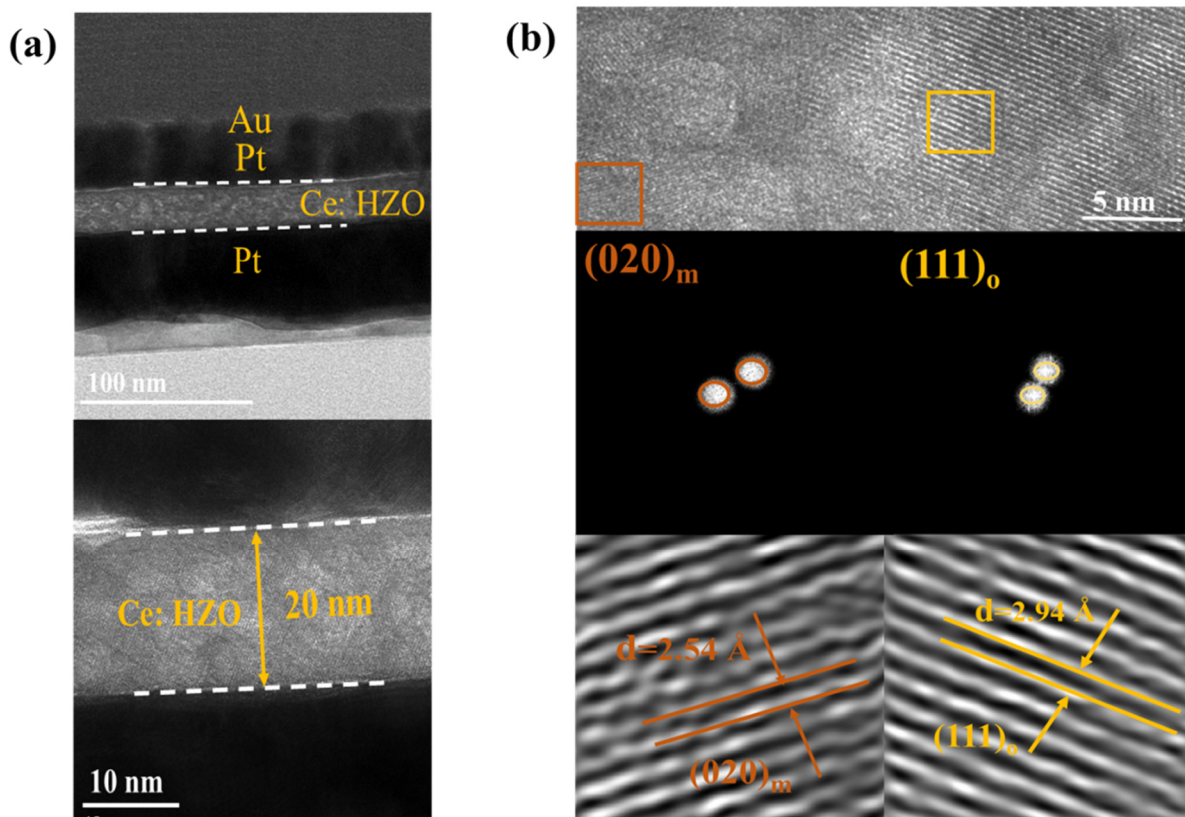


Figure 4. (a) TEM images of the Pt/Ce: HZO/Pt metal–ferroelectric–metal (MIM) structure; (b) cross-sectional HRTEM image of the 7 mol% Ce doping HZO films.

3.2. Electrical Properties of Ce: HZO Thin Films

Figure 5a shows the corresponding P - E hysteresis loop of Ce: $\text{Hf}_{0.5}\text{Zr}_{0.5}\text{O}_2$ thin films with Ce doping concentrations ranging from 0 mol% to 9 mol%. The applied electric field was 2.5 MV/cm. It can be observed that the P - E hysteresis loop shows a small residual polarization at a doping concentration of 0 mol%. The reason for this can be seen in the XRD results presented in Figure 2. In the 0 mol% case, the diffraction peak of $(111)_o$ is not clear, indicating that the stable ferroelectric o phase has not been formed. Thus, the ferroelectricity will be very weak. With an increase in the Ce content to 5 mol%, the film shows a mixed phase consisting of o phase and m phase, and the ferroelectricity gradually appears, showing a residual polarization value of about $13 \mu\text{C}/\text{cm}^2$. Furthermore, when the Ce content reaches 7 mol%, the film exhibits pronounced ferroelectric properties, and the residual polarization value is nearly $17 \mu\text{C}/\text{cm}^2$, which is a remarkable improvement compared with the existing results listed in Table 1. However, with the increase in Ce content to 9 mol%, there is an obvious decrease in the remanent polarization, which can be seen clearly from Figure 5b. This phenomenon can also be understood from the GIXRD results presented in Figure 2. In Figure 2b, an increase in the tetragonal phase and a decrease in the ferroelectric o phase can be observed compared with the 7 mol% case, resulting in a decrease in residual polarization value. In Figure 5b, the values of the coercive field for films different Ce doping concentrations are also presented. In each case, the value of E_c of the Ce: $\text{Hf}_{0.5}\text{Zr}_{0.5}\text{O}_2$ thin films is less than 1.2 MV/cm. The relatively low values of E_c may help to improve the endurance of the thin films.

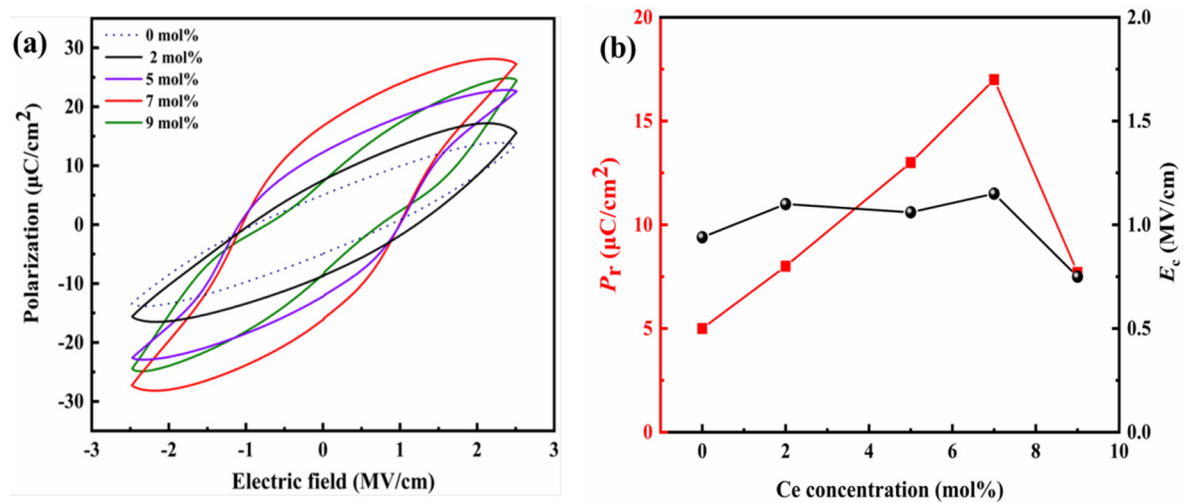


Figure 5. (a) P - E curves and (b) P_r for Ce: HZO thin films with different Ce concentrations.

Testing the relative dielectric constant versus electric field (ϵ_r - E) curve is also an effective method for characterizing the ferroelectric and dielectric properties of thin films [28]. Figure 6a shows Ce: HZO thin films with different doping concentrations. The ϵ_r - E curve is normal for ferroelectrics when the doping concentration is between 0 mol% and 7 mol%. When the doping concentration is 9 mol%, the ϵ_r - E curve presents a double butterfly shape, showing antiferroelectricity characteristics. In previous studies, it has been found that the monoclinic phase of the hafnium oxide ferroelectric film showed a low relative dielectric constant, while the orthogonal phase and cubic phase had a high dielectric constant [13,22,37]. As shown in Figure 6b, with a doping concentration of 0 mol%, the lowest relative dielectric constant can be observed, which may be related to the dominant monoclinic phases in the film, and this phenomenon is consistent with the GIXRD diagram. The monoclinic phase decreases with increasing Ce content, while the high dielectric phase increases obviously, and the relative dielectric constant increases. With the increase in doping concentration, the hysteresis electric field of the film finally stays at about 0.2 MV/cm, which may be due to the change in film uniformity caused by different cerium doping concentrations [38]. These results indicate that the introduction of cerium can promote the uniformity of HZO films.

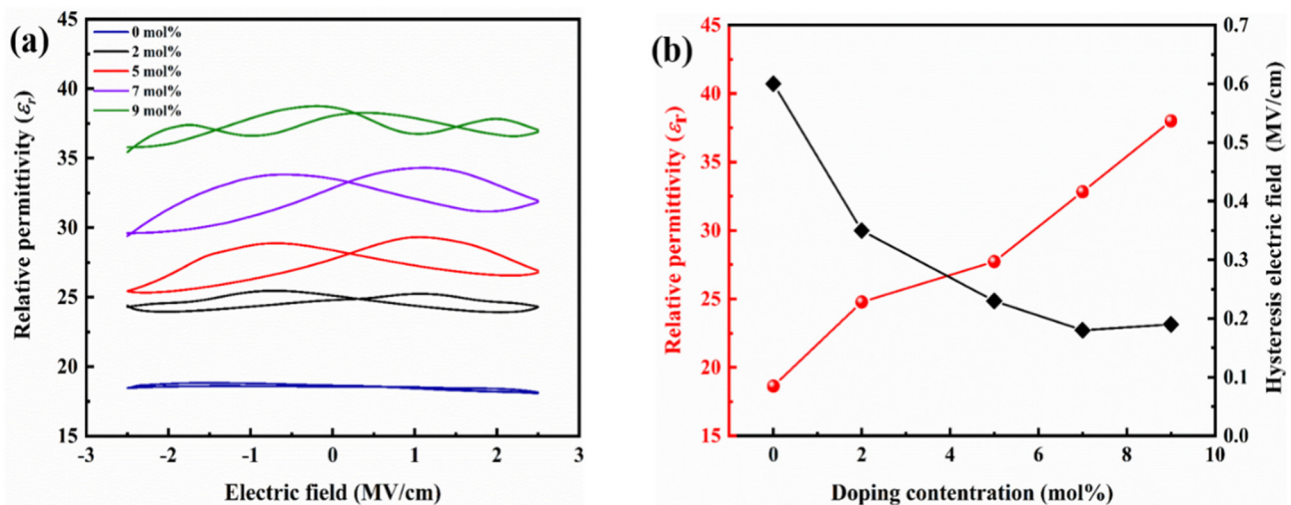


Figure 6. (a) ϵ_r - E curves and (b) hysteresis electric field of Ce: HZO thin films with different Ce concentrations.

The polarization fatigue of the HfO₂ ferroelectric layer is an important factor in determining the lifetime of non-volatile memory devices. Figure 7 shows the endurance properties of Ce: HZO thin films with three different concentrations—0 mol%, 5 mol%, and 7 mol%. The films were cycled with a bipolar square wave at a cycle field of 2.5 MV/cm and a frequency of 500 kHz. Compared with the initial state, there was a slight increase in the polarization before 10⁶ switching cycles. This phenomenon can be attributed to the more uniform distribution of oxygen vacancies, which can reduce the domain wall pinning, and more and more domains are involved in the polarization reversal, leading to an increase in remanent polarization [39,40]. For the pure and 5 mol% concentration HZO thin films, after 10⁸ cycling tests, obvious polarization fatigue was evident, which can be attributed to the cumulative Joule heating and charge trapping effects induced by the leakage current [24]. It is worth mentioning that the Ce: HZO thin films with 7 mol% concentration showed a stable endurance up to 10⁹ bipolar switching cycles, which is better than the results previously reported [41–43]. These experimental results show that doping with cerium can greatly improve the durability of Hf_{0.5}Zr_{0.5}O₂ films.

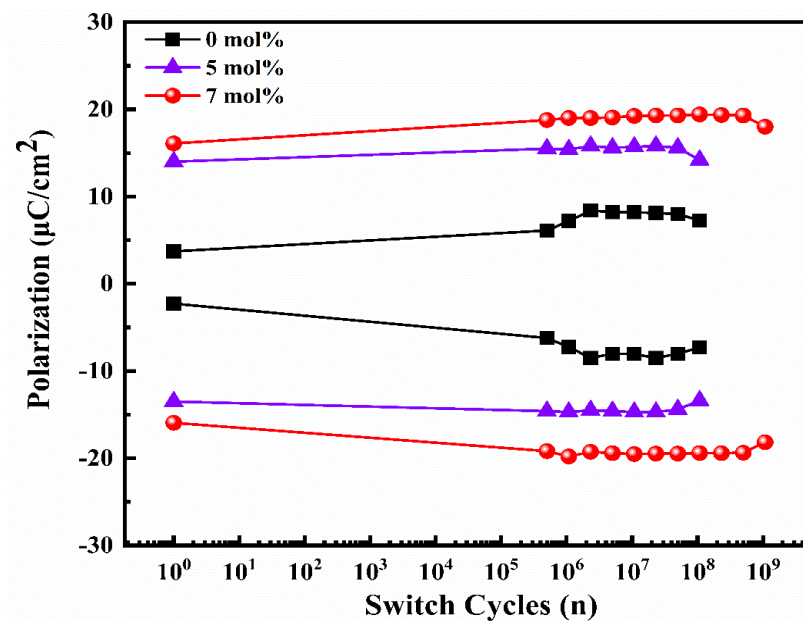


Figure 7. Endurance properties of thin films (0, 5, 7 mol%) at a cycling field of 2.5 MV/cm and a frequency of 500 kHz.

Table 1. Properties of HfO₂-based ferroelectric thin films fabricated by CSD.

Dopant	Remanent Polarization (μC/cm ²)	Coercive Field (MV/cm)	Dopant Concentration (mol%)	Substrate (Bottom Electrode)	Film
Sm	12	(−1.1, +1.6)	5.2	Pt	[11]
(Zr, Y)	15	(−1.4, +1.4)	5	Pt/Ti/SiO ₂ /Si	[23]
(Zr, Sr)	14.6	(−1.1, +1.1)	0.5	Pt/Ti/SiO ₂ /Si	[24]
Zr	8	(−0.8, +0.8)	50	Pt/TiO ₂ /(100) Si	[25]
Pr	6.9	(−1.2, +1.2)	5	Pt/TiO ₂ /(100) Si	[28]
Y	14.2	(+1.4, −1.8)	2	Si (100)	[33]
La	12.5	(−1.1, +1.6)	5.2	Pt	[34]
Y	10	(−1.6, +1.0)	5	Pt	[39]
Ba	12	(−1.7, +1.5)	7.5	Pt/TiO ₂ /SiO ₂	[44]
Ca	5	(−0.9, +0.7)	5.2	Si (100)	[44]
Mg	3	(−0.8, +0.8)	7.5	Pt/TiO ₂ /SiO ₂	[44]
(Zr, Ce)	17	(−1.2, +1.1)	7	Pt/Ti/SiO ₂ /Si	This work

4. Conclusions

In summary, Ce: Hf_{0.5}Zr_{0.5}O₂ thin films were successfully prepared by chemical solution deposition. The XPS results showed that appropriate Ce doping can introduce a certain amount of oxygen vacancies, which helps to form the ferroelectric o phase. In addition, Ce doping can improve the dielectric properties and uniformity of HZO films. In the Ce: Hf_{0.5}Zr_{0.5}O₂ thin film with a doping concentration of 7 mol%, a stable ferroelectric o phase was formed, and the residual polarization value reached 17 $\mu\text{C}/\text{cm}^2$. Meanwhile, after 10⁹ bipolar switching cycles, the film showed good endurance, and only slight degradation of polarization. The results show that cerium doping can improve the ferroelectric properties and durability of Hf_{0.5}Zr_{0.5}O₂ thin films.

Author Contributions: Writing—original draft preparation, Y.-G.X. and S.-W.L.; writing—review and editing, L.-S.Y., Y.J., K.X., G.L., J.O. and M.-H.T. All authors have read and agreed to the published version of the manuscript.

Funding: This research was funded by the cultivation projects of the National Major R & D Project (grant no. 92164108), the National Natural Science Foundation of China under Grant Nos. 51872250, and 11835008, the technology innovation leading plan (Science and technology tackling) project of Hunan Provincial new and high-tech industry under Grant No. 2020GK2052, the State Key Laboratory of Intense Pulsed Radiation Simulation and Effect (North west Institute of Nuclear Technology) under Grant No. SKLIPR1814, the Foundation of Innovation Center of Radiation Application (grant no. KFZC2020020901), and the Key Laboratory of Low Dimensional Materials & Application Technology of Ministry of Education (Xiangtan University) under Grant No. KF20180203.

Institutional Review Board Statement: Not applicable.

Informed Consent Statement: Not applicable.

Data Availability Statement: All data included in this study are available upon request by contact with the corresponding author.

Conflicts of Interest: The authors declare no conflict of interest.

References

1. Hu, Y.Q.; Wang, C.H.; Dong, H.; Wallace, R.M.; Cho, K.; Wang, W.H.; Wang, W.C. Origin of indium diffusion in high-k oxide HfO₂. *ACS Appl. Mater. Interfaces* **2016**, *8*, 7595–7600. [[CrossRef](#)] [[PubMed](#)]
2. Tirmali, P.M.; Khairnar, A.G.; Joshi, B.N.; Mahajanl, A.M. Structural and electrical characteristics of RF-sputtered HfO₂ high-k based MOS capacitors. *Solid-State Electron.* **2011**, *62*, 44–47. [[CrossRef](#)]
3. Böske, T.S.; Müller, J.; Bräuhäus, D.; Schröder, U.; Böttger, U. Ferroelectricity in hafnium oxide thin films. *Appl. Phys. Lett.* **2011**, *99*, 102903. [[CrossRef](#)]
4. Khan, A.I.; Keshavarzi, A.; Datta, S. The future of ferroelectric field-effect transistor technology. *Nat. Electron.* **2020**, *3*, 588–597. [[CrossRef](#)]
5. Park, M.H.; Lee, Y.H.; Mikolajick, T.; Schroeder, U. Review and perspective on ferroelectric HfO₂-based thin films for memory applications. *MRS Commun.* **2018**, *8*, 795–808. [[CrossRef](#)]
6. Olsen, T.; Schröder, U.; Müller, S.; Krause, A.; Martin, D.; Singh, A.; Müller, J. Co-sputtering yttrium into hafnium oxide thin films to produce ferroelectric properties. *Appl. Phys. Lett.* **2012**, *101*, 082905. [[CrossRef](#)]
7. Mueller, S.; Mueller, J.; Singh, A.; Riedel, S.; Sundqvist, J.; Schroeder, U.; Mikolajick, T. Incipient ferroelectricity in Al-doped HfO₂ thin films. *Adv. Funct. Mater.* **2012**, *22*, 2412–2417. [[CrossRef](#)]
8. Chouprik, A.; Chernikova, A.; Markeev, A.; Mikheev, V.; Negrov, D.; Spiridonov, M.; Zarubin, S.; Zenkevich, A. Electron transport across ultrathin ferroelectric Hf_{0.5}Zr_{0.5}O₂ films on Si. *Microelectron. Eng.* **2017**, *178*, 250–253. [[CrossRef](#)]
9. Wei, A.Q.; Chen, C.; Tang, L.; Zhou, K.C.; Zhang, D. Chemical solution deposition of ferroelectric Sr: HfO₂ film from inorganic salt precursors. *J. Alloys Compd.* **2018**, *731*, 546–553. [[CrossRef](#)]
10. Sourav, D.; Han, Q.B.; Bu, W.X.; Baig, M.A.; Sung, P.J.; Su, C.J.; Lee, Y.J.; Lu, D.D. Uniform crystal formation and electrical variability reduction in hafnium-oxide-based ferroelectric memory by thermal engineering. *ACS Appl. Electron. Mater.* **2021**, *3*, 619–628.
11. Starschich, S.; Griesche, D.; Schneller, T.; Böttger, U. Chemical solution deposition of ferroelectric hafnium oxide for future lead free ferroelectric devices. *ECS J. Solid State Sci. Technol.* **2015**, *4*, P419. [[CrossRef](#)]
12. Tromm, T.C.U.; Zhang, J.; Schubert, J.; Luysberg, M.; Zander, W.; Han, Q.; Meuffels, P.; Meertens, D.; Glass, S.; Bernardy, P.; et al. Ferroelectricity in Lu doped HfO₂ layers. *Appl. Phys. Lett.* **2017**, *111*, 142904. [[CrossRef](#)]

13. Mehmood, F.; Mikolajick, T.; Schroeder, U. Lanthanum doping induced structural changes and their implications on ferroelectric properties of $\text{Hf}_{1-x}\text{Zr}_x\text{O}_2$ thin film. *Appl. Phys. Lett.* **2020**, *117*, 092902. [[CrossRef](#)]
14. Schroeder, U.; Yurchuk, E.; Müller, J.; Martin, D.; Schenk, T.; Polakowski, P. Impact of different dopants on the switching properties of ferroelectric hafniumoxide. *Jpn. J. Appl. Phys.* **2014**, *53*, 08LE02. [[CrossRef](#)]
15. Shimizu, T.; Yokouchi, T.; Shiraishi, T.; Oikawa, T. Study on the effect of heat treatment conditions on metalorganic-chemical-vapor-deposited ferroelectric $\text{Hf}_{0.5}\text{Zr}_{0.5}\text{O}_2$ thin film on Ir electrode. *Jpn. J. Appl. Phys.* **2014**, *53*, 09PA04. [[CrossRef](#)]
16. Liu, B.W.; Zhang, Y.R.; Zhang, L.J.; Yuan, Q.T.; Zhang, W.; Li, Y.B. Excellent HZO ferroelectric thin films on flexible PET substrate. *J. Alloys Compd.* **2022**, *919*, 165872. [[CrossRef](#)]
17. Lederer, M.; Bagul, P.; Lehninger, D.; Mertens, K.; Reck, A.; Olivo, R. Influence of annealing temperature on the structural and electrical properties of Si-doped ferroelectric hafnium oxide. *ACS Appl. Electron. Mater.* **2021**, *3*, 4115–4120. [[CrossRef](#)]
18. Ali, T.; Olivo, R.; Kerdilès, S.; Lehninger, D.; Lederer, M.; Sourav, D.; Royet, A.-S.; Sünbül, A.; Prabhu, A.; Kühnel, K.; et al. Study of nanosecond laser annealing on silicon doped hafnium oxide film crystallization and capacitor reliability. In Proceedings of the 2022 IEEE International Memory Workshop (IMW), Dresden, Germany, 15–18 May 2022; pp. 1–4.
19. Wang, D.; Zhang, Y.; Wang, J.L.; Luo, C.L.; Li, M.; Shuai, W.T.; Tao, R.Q.; Fan, Z.; Chen, D.Y.; Zeng, M. Enhanced ferroelectric polarization with less wake-up effect and improved endurance of $\text{Hf}_{0.5}\text{Zr}_{0.5}\text{O}_2$ thin films by implementing W electrode. *J. Mater. Sci. Technol.* **2022**, *104*, 1–7. [[CrossRef](#)]
20. Payne, A.; Hsain, H.A.; Lee, Y.; Strnad, A.N.; Jones, L.J.; Hanrahan, B. Thermal stability of antiferroelectric-like Al: HfO_2 thin films with TiN or Pt electrodes. *Appl. Phys. Lett.* **2022**, *120*, 232901. [[CrossRef](#)]
21. Katayama, K.; Shimizu, T.; Sakata, O.; Shiraishi, T.; Nakamura, S.; Kiguchi, T.; Akama, A.; Konno, J.T.; Uchida, H.; Funakubo, H. Orientation control and domain structure analysis of {100}-oriented epitaxial ferroelectric orthorhombic HfO_2 -based thin films. *J. Appl. Phys.* **2016**, *119*, 134101. [[CrossRef](#)]
22. Kozodaev, M.G.; Chernikova, A.G.; Korostylev, E.V.; Park, M.H.; Khakimov, R.R.; Hwang, C.S.; Markeev, A.M. Mitigating wake-up effect and improving endurance of ferroelectric HfO_2 - ZrO_2 thin films by careful La-doping. *J. Appl. Phys.* **2019**, *125*, 034101. [[CrossRef](#)]
23. Mohit, T.M.; Haga, K.I.; Eisuke, T. Impact of annealing environment on electrical properties of yttrium-doped hafnium zirconium dioxide thin films prepared by the solution process. *Jpn. J. Appl. Phys.* **2020**, *59*, SPPB03. [[CrossRef](#)]
24. Yin, L.; Gong, S.Q.; Li, X.Y.; Lu, B.B.; Peng, Q.X.; Zheng, S.Z.; Liao, M.; Zhou, Y.C. Improvement of ferroelectricity and endurance in Sr doped $\text{Hf}_{0.5}\text{Zr}_{0.5}\text{O}_2$ films. *J. Alloys Compd.* **2022**, *914*, 165301. [[CrossRef](#)]
25. Shuhei, N.; Hiroshi, F.; Hiroshi, U. Crystallization behavior and ferroelectric property of HfO_2 - ZrO_2 films fabricated by chemical solution deposition. *Jpn. J. Appl. Phys.* **2018**, *57*, 11UF06.
26. Künneth, C.; Materlik, R.; Falkowski, M.; Kersch, A. Impact of Four-Valent Doping on the Crystallographic Phase Formation for Ferroelectric HfO_2 from First-Principles: Implications for Ferroelectric Memory and Energy-Related Applications. *ACS Appl. Nano Mater.* **2018**, *1*, 254–264. [[CrossRef](#)]
27. Zheng, S.Z.; Zhao, Z.D.; Liu, Z.T.; Zeng, B.J.; Yin, L.; Peng, Q.X.; Liao, M.; Zhou, Y.C. Improvement of remanent polarization of CeO_2 - HfO_2 solid solution thin films on Si substrates by chemical solution deposition. *Appl. Phys. Lett.* **2020**, *117*, 212904. [[CrossRef](#)]
28. Liu, H.; Zheng, S.Z.; Chen, Q.; Zeng, B.J.; Jiang, J.; Peng, Q.X.; Liao, M.; Zhou, Y.C. Structural and ferroelectric properties of Pr doped HfO_2 thin films fabricated by chemical solution method. *J. Mater. Sci. Mater. Electron.* **2019**, *30*, 5771–5779. [[CrossRef](#)]
29. Shibayama, S.; Nagano, J.; Asaka, K.; Sakashita, M.; Nakatsuka, O. Impact of Wet Annealing on Ferroelectric Phase Formation and Phase Transition of HfO_2 - ZrO_2 System. *ACS Appl. Electron. Mater.* **2021**, *3*, 2203–2211. [[CrossRef](#)]
30. Falkowski, M.; Kersch, A. Optimizing the piezoelectric strain in ZrO_2 and HfO_2 -Based incipient ferroelectrics for thin-film applications: An ab initio dopant screening study. *ACS Appl. Mater. Interfaces* **2020**, *12*, 32915–32924. [[CrossRef](#)]
31. Avis, C.; Kim, Y.G.; Jang, J. Solution processed hafnium oxide as a gate insulator for low-voltage oxide thin-film transistors. *J. Mater. Chem.* **2012**, *22*, 17415–17420. [[CrossRef](#)]
32. Pan, T.M.; Lu, C.H. Switching behavior in rare-earth films fabricated in full room temperature. *IEEE Trans. Electron Devices* **2012**, *59*, 956–961. [[CrossRef](#)]
33. Wang, X.X.; Zhou, D.Y.; Li, S.D.; Liu, X.H.; Zhao, P.; Sun, N.; Ali, F.; Wang, J.J. Ferroelectric yttrium doped hafnium oxide films from all-inorganic aqueous precursor solution. *Ceram. Int.* **2018**, *44*, 13867–13872. [[CrossRef](#)]
34. Islamov, D.R.; Zalyalov, T.M.; Orlov, O.M.; Gritsenko, V.A.; Krasnikov, G.Y. Impact of oxygen vacancy on the ferroelectric properties of lanthanum-doped hafnium oxide. *Appl. Phys. Lett.* **2020**, *117*, 162901. [[CrossRef](#)]
35. Hsain, H.A.; Lee, Y.H.; Parsons, G. Compositional dependence of crystallization temperatures and phase evolution in hafnia-zirconia ($\text{Hf}_{1-x}\text{Zr}_x$) O_2 thin films. *Appl. Phys. Lett.* **2020**, *116*, 192901. [[CrossRef](#)]
36. Xiao, W.W.; Liu, C.; Peng, Y.; Zheng, S.Z.; Zhang, C.F.; Liao, M.; Zhou, Y.C. Performance improvement of $\text{Hf}_{0.5}\text{Zr}_{0.5}\text{O}_2$ -based ferroelectric-field-effect transistors with ZrO_2 seed layers. *IEEE Electron Device Lett.* **2019**, *40*, 714–717. [[CrossRef](#)]
37. Hoffmann, M.; Schroeder, U.; Schenk, T.; Shimizu, T.; Funakubo, H.; Sakata, O.; Pohl, D.; Drescher, M.; Adelman, C.; Materlik, R.; et al. Stabilizing the ferroelectric phase in doped hafnium oxide. *J. Appl. Phys.* **2015**, *118*, 072006. [[CrossRef](#)]
38. Zhao, Y.P.; Wang, G.C.; Lu, T.M.; Palasantzas, G.; De Hosson, J.T.M. Surface-roughness effect on capacitance and leakage current of an insulating film. *Phys. Rev. B* **1999**, *60*, 9157. [[CrossRef](#)]

39. Fields, S.S.; Smith, S.W.; Ryan, P.J.; Jaszewski, I.A.; Alejandro, S.B.; Esteves, G.; Steve, L. Phase-exchange-driven wake-up and fatigue in ferroelectric hafnium zirconium oxide films. *ACS Appl. Mater. Interfaces* **2020**, *12*, 26577–26585. [[CrossRef](#)]
40. Starschich, S.S.; Menzel, S.; Böttger, U. Evidence for oxygen vacancies movement during wake-up in ferroelectric hafnium oxide. *Appl. Phys. Lett.* **2016**, *108*, 032903. [[CrossRef](#)]
41. Song, T.F.; Tan, H.; Estandía, S.; Gàzquez, J.; Gich, M. Improved polarization and endurance in ferroelectric Hf_{0.5}Zr_{0.5}O₂ films on SrTiO₃ (110). *Nanoscale* **2022**, *14*, 2337–2343. [[CrossRef](#)]
42. Kim, S.J.; Mohan, J.; Summerfelt, S.R.; Kim, J. Ferroelectric Hf_{0.5}Zr_{0.5}O₂ thin films: A review of recent advances. *JOM* **2019**, *71*, 246–255. [[CrossRef](#)]
43. Lyu, J.; Song, T.F.; Fina, I.; Sánchez, F. High polarization, endurance and retention in sub-5 nm Hf_{0.5}Zr_{0.5} O₂ films. *Nanoscale* **2020**, *12*, 11280–11287. [[CrossRef](#)] [[PubMed](#)]
44. Starschich, S.; Boettger, U. An extensive study of the influence of dopants on the ferroelectric properties of HfO₂. *J. Mater. Chem. C* **2017**, *5*, 333–338. [[CrossRef](#)]